

Distribution and characteristics of Infrared Dark Clouds using genetic forward modelling

D.J. Marshall and G. Joncas

*Département de physique, de génie physique et d'optique et Centre de recherche en astrophysique du Québec,
Université Laval, Québec, QC, G1V 0A6, Canada*

and

A.P. Jones

Institut d'Astrophysique Spatiale, bâtiment 121, Université Paris-XI, Orsay, 91405, France

ABSTRACT

Infrared Dark Clouds (IRDCs) are dark clouds seen in silhouette in mid-infrared surveys. They are thought to be the birthplace of massive stars, yet remarkably little information exists on the properties of the population as a whole (e.g. mass spectrum, spatial distribution). Genetic forward modelling is used along with the Two Micron All Sky Survey and the Besançon Galactic model to deduce the three dimensional distribution of interstellar extinction towards previously identified IRDC candidates. This derived dust distribution can then be used to determine the distance and mass of IRDCs, independently of kinematic models of the Milky Way. Along a line of sight that crosses an IRDC, the extinction is seen to rise sharply at the distance of the cloud. Assuming a dust to gas ratio, the total mass of the cloud can be estimated.

The method has been successfully applied to 1259 IRDCs, including over 1000 for which no distance or mass estimate currently exists. The IRDCs are seen to lie preferentially along the spiral arms and in the molecular ring of the Milky Way, reinforcing the idea that they are the birthplace of massive stars. Also, their mass spectrum is seen to follow a power law with an index of -1.75 ± 0.06 , steeper than giant molecular clouds in the inner Galaxy, but comparable to clumps in GMCs. This slope suggests that the IRDCs detected using the present method are not gravitationally bound, but are rather the result of density fluctuations induced by turbulence.

Subject headings: dust, extinction - Galaxy: structure - ISM: clouds - infrared: ISM

1. Introduction

The first reported detection of Infrared Dark Clouds (IRDCs) was by Perault (1996), who noted regions in mid-infrared (MIR) ISOCAM observations that were optically thick at $15 \mu\text{m}$. Egan et al. (1998) noted that many of these dark features do not emit significantly in the far-infrared, implying that they are cold ($< 20 \text{ K}$) and dense ($n > 10^5 \text{ cm}^{-3}$) molecular clouds.

There has been much interest recently in IRDCs, as they are thought to be the initial phase of massive star formation. Indeed, active star formation has been detected in a number of dense IRDCs

(Ormel et al. 2005; Rathborne et al. 2005; Pillai et al. 2006; Chambers et al. 2009). In order to obtain more information on the clouds themselves as a population, Simon et al. (2006a) analysed MIR images from the Midcourse Space Experiment (MSX, Price 1995). They searched for contiguous regions of high decremental contrast with respect to the MIR background and they identified over 10000 IRDC candidates in the first and fourth Galactic quadrants. In a subsequent study, Simon et al. (2006b) used ^{13}CO observations to determine kinematic distances to and masses of over 300 of the IRDC candidates. Rathborne et al. (2006) used the kinematic distances determined by

Simon et al. (2006b) along with dust continuum observations and determined the masses of nearly 40 IRDCs. More recently, Jackson et al. (2008) used CS observations to determine the kinematic distances to over 300 4th quadrant IRDCs. The typical size of the IRDCs found by the above authors is 5 pc, their average mass is $\sim 3 \times 10^3 M_\odot$, and their distances indicate that they lie preferentially in the molecular ring of the Galaxy (Simon et al. 2006b; Jackson et al. 2008). The mass spectra for the IRDCs is found to follow a power law, with a spectral index steeper than that found for Giant Molecular Clouds in the inner Galaxy (Simon et al. 2006b). The cores within the IRDCs, however, are steeper still and are very close to the Salpeter IMF (Rathborne et al. 2006).

The area of the Galaxy where the detection of IRDCs is easiest, namely inside the solar circle due to the high MIR background, is also the region where distance determinations are the most problematic. Tackling the problem from a variety of angles is therefore very important in order to avoid introducing bias. In order to extend and complement the latest findings on the Galactic distribution of IRDCs, a new tridimensional extinction mapping method is used to locate their positions and line of sight extinctions. Stars observed in the near infrared are compared to a Galactic Population Synthesis model (Robin et al. 2003), and the extinction required to redden the modelled stars to match the observed stars is found via a genetic algorithm (GA, Charbonneau 1995). Near infrared data are well suited to study these IRDC candidates as K_s band extinction is only a factor of two higher than the extinction at $8 \mu\text{m}$ (Indebetouw et al. 2005).

In section 2 we describe the observations and model used to calculate the extinction. In section 3 we describe how we determine the line of sight extinction to IRDC candidates, and how this information is converted to a distance and mass estimate for the cloud. We describe the results in section 4 and discuss the implications in section 5. We conclude in section 6.

2. Model and observations

2.1. Two Micron All Sky Survey

The Two Micron All Sky Survey (2MASS, Skrutskie et al. 2006) is a ground based survey which uniformly scanned the entire sky in three near-infrared bands (J , H & K_s). Amongst its final products is the point source catalogue (PSC) which includes point sources brighter than about 1 mJy in each band, with signal-to-noise

ratio (SNR) greater than 10, using a pixel size of $2.0''$. It is complete down to a limiting magnitude of 15.7, 15.1 and 14.3 in the J , H and K_s bands, respectively, and in the absence of confusion.

2.2. The Galactic model

The stellar population synthesis model of the Galaxy constructed in Besançon (Robin et al. 2003), hereafter called the Galactic model, is able to simulate the stellar content of the Galaxy by modelling four distinct stellar populations: the thin disc, the thick disc, the outer bulge and the spheroid. It also takes into account the dark halo and a diffuse component of the interstellar medium. It can be used to generate stellar catalogues for any given direction, and returns information on each star such as magnitude, colour, and distance as well as kinematics and other stellar parameters.

The approach of the Galactic model is semi-empirical as it is based on theoretical grounds (for example stellar evolution, galactic evolution and galactic dynamics) and is constrained by empirical observations (the local luminosity function for example). The Galactic potential is calculated in order to self-consistently constrain the disc scale height. In addition, the model simulates photometric errors and includes Poisson noise to make it ideal for direct comparison with observations.

The Galactic model has been used for various studies, such as identification of Galactic structures through stellar overdensities (Picaud et al. 2003; Bellazzini et al. 2004; Momany et al. 2004), Galactic parameter estimation from fitting model to observations (Picaud & Robin 2004; Reyl   et al. 2009) as well as the quantification of the uncertainty in extinction estimation (Froebich & del Burgo 2006) to name but a few. Many more examples are given in Robin et al. (2003).

2.3. Comparing model to observations

The Galactic model has been developed to return results in the near-infrared and visible filters, and is a powerful tool to extract the extinction information embedded in the 2MASS observations (Marshall et al. 2006).

However, the PSC can be compared quantitatively with the Galactic model simulations only where the former is shown to be complete. As such, we must compute the faint completeness limit field by field. We

do so by creating magnitude histograms in each band and locating the faintest magnitude where the source counts are still increasing linearly. We use a bright cutoff of 10 in all three bands, as recommended in the online explanatory supplement¹. In order to closely model the 2MASS stars, we cut the modelled stars at the 2MASS completeness limits and simulate the photometric errors via an exponential function which is able to reproduce typical CCD photometric errors very well.

3. Method

The method used to determine the distance and extinction to the IRDCs is based on a modified version of the three dimensional extinction method first described in Marshall et al. (2006). The base of the extinction method remains a comparison of the stellar colours of the Galactic model and the 2MASS dataset, as extinction gives rise to a colour excess. For example, for the J and K_s bands the colour excess is:

$$E(J - K_s) = (J - K_s) - (J - K_s)_0 \quad (1)$$

where the 0 subscript denotes intrinsic colour. This equation can be rewritten as:

$$E(J - K_s) = (J - J_0) - (K_s - K_{s0}) = A_J - A_{K_s} \quad (2)$$

as the extinction in a given band is just the difference between observed and unreddened apparent magnitude. Putting these relations together, we can write:

$$A_{K_s} = R_{JK} E(J - K_s) \quad (3)$$

where $R_{JK} = (1/(A_J/A_{K_s} - 1))$ is the ratio of absolute to relative extinction. The modifications to the basic method are described below.

3.1. Genetic algorithm approach

In Marshall et al. (2006) the authors calculate the extinction via the colour difference between observed reddened stars and simulated unreddened ones (i.e. to which no extinction correction has been applied). The distance information is then obtained by assuming that more distant stars are redder, as interstellar extinction in a monotonically growing function with distance. This is true for the giant star population only, so dwarf stars are excluded from the calculation.

An alternative is to turn the problem on its head. Instead of calculating an extinction based on colour differences between observed and modelled stars, one can generate a large number of extinction distributions and keep the one that results in a good fit between observed and modelled stars. An immediate advantage of this method is that the information from all of the stars is used, not just the giants. However the sheer number of possible solutions prevents us from applying a “brute force” approach. We have instead applied the genetic algorithm (GA) approach described in Charbonneau (1995).

In essence the GA generates and tests different extinction distributions towards a candidate IRDC, defined as a number of points each with a distance and a corresponding extinction. The extinction is thus no longer calculated, but is an output from the GA. For each generated extinction distribution, the modelled stars are reddened using Eq.3, and the goodness of fit between the observed and simulated stellar colour distributions is calculated via a merit function, described below. Initially, a “population” of random solutions is generated. Solutions in this group with the highest values of the merit function are combined to produce “child” solutions in a new “generation” of solutions. This evolution is allowed to continue for at most 500 generations after which the fittest solution found is retained. If the solution converges before then, defined as 25 generations with no improvement in the fittest individual, the iteration is stopped and the fittest solution found up to that point is adopted.

The use of Galactic modelling and GAs to solve for three dimensional extinction is an interesting alternative to other techniques, as no single stellar population need be isolated, and there is no such thing as foreground contamination - all stars are used in the extinction calculation. However these advantage comes at a price - high CPU use resulting in a long execution time. Each point along a line of sight towards the IRDC, and contained within its defining ellipse, corresponds to two parameters (distance and extinction) and so by reducing the number of parameters to fit, a substantial gain in time is possible. This is done by fixing the extinction values on a regular grid along each line of sight and searching only for the corresponding distance to each extinction value. This approach is superior to fixing the distance to a regular grid, as sharp rises in extinction are easier to identify.

The extinction values along the line of sight are thus

¹http://www.ipac.caltech.edu/2mass/releases/allsky/doc/sec6_5a1.html

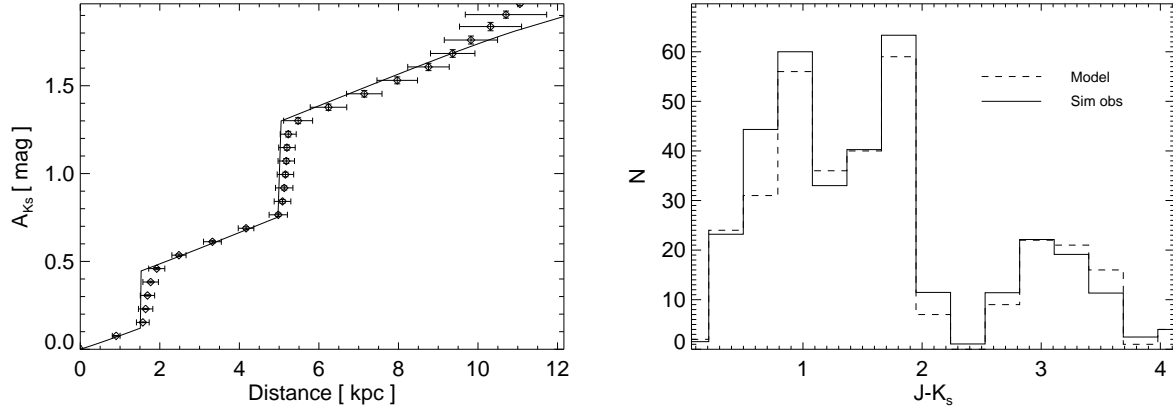


Fig. 1.— **Left:** Extinction distribution for an example line of sight. The observations have been simulated using the Galaxy model with known extinction distribution (solid line). Note that the distance error bars generally increase with distance. **Right:** Colour histogram for the $J-K_s$ colour index for the simulated observations (solid line) and the model adjusted with the extinction points of figure on the left.

equally spaced:

$$A_{K_s}(i) = i \times \delta A_{K_s} \quad (4)$$

for each line of sight point i and where δA_{K_s} is taken to be twice the minimum extinction detectable. Assuming that the minimum extinction detectable arises from the uncertainty in the 2MASS $J-K_s$ colour, this value is then, using Eq.3:

$$\delta A_{K_s} = 2 * \frac{\sqrt{(\Delta J^2 + \Delta K_s^2)}}{(A_J/A_{K_s}) - 1} \quad (5)$$

where ΔJ and ΔK_s are the average uncertainty in the magnitude of the J and K_s bands, respectively. Typically, this corresponds to $0.06 \lesssim \delta A_{K_s} \lesssim 0.1$. The distribution of photometric errors is Poissonian, requiring the use of the mean in the above equation so as to not allow the extinction calculation to work purely on noise. Also, the use of the $J-K_s$ colour index is justifiable as it is the most sensitive of the three to interstellar extinction.

The distance values along the line of sight are:

$$r_i = r_{i-1} + \delta r_i \quad i > 1 \quad (6)$$

where $r_1 = 0$ and the δr_i are the variables that are searched for using the GA.

We have added two modifications to this schema. First of all, a crude estimate to the solution is estimated by finding a smooth extinction solution. The Galactic

dust distribution in the model is approximated using a double exponential disc with an *ad hoc* local normalisation. The best local normalisation is found in order to minimise the χ^2 difference between observed and modelled stellar colour distributions for the particular line of sight. This rough solution is inserted into the initial population as an “alpha male”, intended to get the GA looking in the right direction. This “alpha male” is generally replaced by a fitter solution within the first couple of generations and does not influence the final solution, but greatly reduces the convergence time. If the initial random generation of solutions contains a fitter individual than the alpha male is not used.

Secondly we have modified one of the reproduction functions used to create child solutions, namely the crossover operator. GAs encode the solutions into individual strings called genotypes. In our case the solution is a series of δr_i values (Eq.6) which the GA normalises. A simple example consisting of two points which we describe to three decimal digits would then be a six digit number. The crossover operator would take two parent genotypes, randomly select a digit to perform the cut, and then simply swap the remaining digits between the two parents to create two new children. This singular cut results in a slower mixing of the genotypes so we have changed it to N-point crossover. In this scheme, the number of cuts is a random variable and so the children contain more diversity than in the simple crossover operator. This approach emphasises

exploration of the parameter space, with less exploitation of the fittest individual. We are not looking for a high precision solution as the colour distribution of the observations can be reproduced with a spread of extinction solutions (see Sect.3.3). Rather we want to avoid any secondary, local minima in the χ^2 minimisation.

3.2. Merit function

For each line of sight we are comparing observed stars with simulated stars from the Galactic model via the histograms of their respective colour indices ($J - K_s$ and $H - K_s$). We calculate their difference using a χ^2 statistic, where higher merit is associated with a lower value of the χ^2 statistic. However, if the Galactic model overestimates or underestimates the number of stars along a particular line of sight we do not want this to influence the extinction we measure. Consider a hypothetical case where the model predicts a factor of two too many stars. If we were to use a standard χ^2 test between modelled and observed colour distribution, then the extinction we find could be artificially boosted in order to remove a number of simulated stars by pushing them beyond the completeness limit for the line of sight. This is obviously an unacceptable situation.

To avoid this “artificial extinction” the merit function used is based on a normalised χ^2 test from Press et al. (1992) :

$$\chi^2 = \sum_i \frac{(\sqrt{N_o/N_m} n_{m_i} - \sqrt{N_m/N_o} n_{o_i})^2}{n_{m_i} + n_{o_i}} \quad (7)$$

where n_{o_i} (N_o) and n_{m_i} (N_m) are the number of stars in the i^{th} bin of the colour histogram (total number of stars along the line of sight) of the observations and model, respectively. The term involving the total number of stars ensures that the χ^2 statistic will be lowest when the shapes of the two histograms are the same, regardless of any difference in the total number of stars. To ensure the best fit, the $J - K_s$ and $H - K_s$ colour indices are adjusted simultaneously. If only one is used, the GA will find the optimum solution for that colour index, perhaps at the expense of one of the others. An example line of sight is presented in the left hand side of Fig.1 using simulated observations from the Galactic model. The simulated observations contain a diffuse extinction component (of $0.7 A_V \text{ kpc}^{-1}$) along with two clouds at 1.5 and 5 kpc with extinctions of 0.34 and 0.57 magnitudes in the K_s band respectively. The stellar density and extinctions used in the

simulation is typical of that seen for the IRDCs. The histograms of the $J - K_s$ colour index are shown on the right side of Fig.1 for the simulated observations (solid line) and the Galactic model reddened using the points shown on the left hand side of Fig.1. The GA is seen to find the diffuse extinction as well as both clouds. The detection of the clouds and the determination of their characteristics will be discussed in section 3.4 below.

3.3. Error estimation

The random nature of the GA means that two subsequent calculations along the same line of sight will not be identical. Furthermore, the Besançon model generates simulated stars using density distributions and luminosity functions, meaning that generating a simulated stellar catalogue twice for the same line of sight will not result in the same exact solution either. However, by rerunning the Galactic model and repeating the extinction calculation a number of times and taking the mean, a more robust estimator of the extinction distribution can be obtained. The variation in the solutions found provide us with a measure of the uncertainty, as they provide a range of extinction solutions which are able to fit the model to the observations.

Each iteration to calculate the extinction along the line of sight is a lengthy process and we wish to minimise the number of iterations while still performing enough to obtain a robust mean. In order to determine the number of solutions which should be generated, we calculated the extinction for a few lines of sight 300 times. It was found that there was no difference in the mean after 100 and after 300 iterations, so we assume that the method has converged at 100 iterations and that we have found the best solution and associated uncertainty. This number of iterations would require a very lengthy calculation for the thousands of candidate IRDCs so we searched for the minimum number of iterations which satisfactorily reproduced the result found after 100 iterations. The results of this test for one line of sight is presented in Fig.2. The black solid line with the grey shaded area represent the mean and the standard deviation, respectively, after 100 iterations. From left to right, and top to bottom we display the results after 3, 5, 10 and 15 iterations. As can be seen, there is far too much variation in the mean for iterations less than 15. After 15 iterations, the mean and standard deviations are very close to those obtained after 100 iterations. We thus proceed using only 15 iterations.

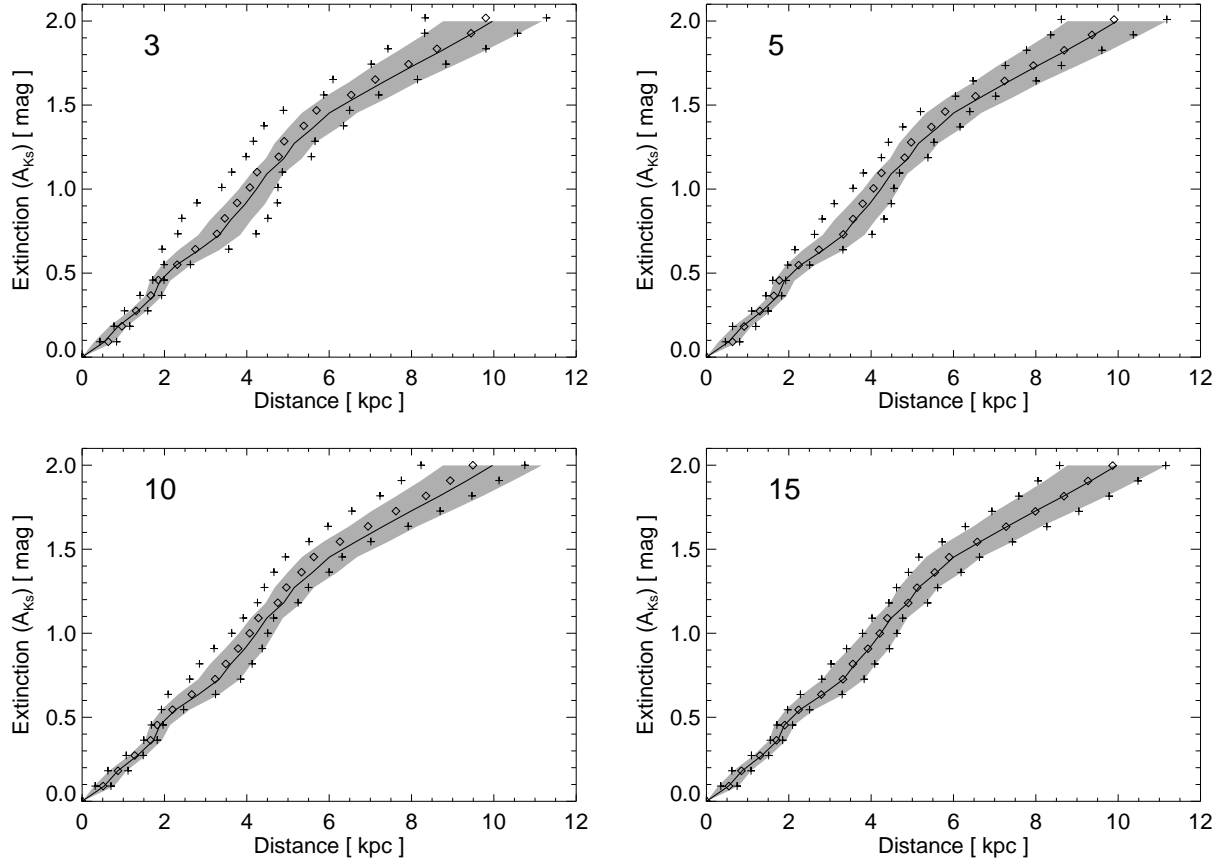


Fig. 2.— Extinction along a test line of sight at $l = 50^\circ$ $b = 0^\circ$. Each figure shows the resulting extinction after averaging a different number of calculations. The solid line and grey shaded area show the average and standard deviation after 100 runs. The diamonds show the mean and the crosses show the standard deviation after the number of runs showed in the top left corner.

3.4. Cloud identification and properties

Clouds for which we attempt to measure their extinction come from a catalogue of IRDC candidates from (Simon et al. 2006a). In this catalogue the IRDCs are defined as contiguous regions of MIR extinction. The catalogue defines ellipses enclosing the clouds and supplies their position, major and minor axes, position angle as well as peak contrast and area. For each cloud we fetch the 2MASS observations within the ellipse. All clouds which contain over 50 observed stars in J , H and K_s are retained. We require all three magnitudes in order to calculate the various colour indices. There is a large spread in stellar colours towards the dark clouds and we require at least five stars in each colour histogram bin to calculate a

meaningful χ^2 statistic. The lower bound of 50 stars is chosen somewhat arbitrarily in order to ensure the colour histograms have a sufficient number of stars per bin. The line of sight extinction towards this ellipse is then calculated. In Fig.3, an example ellipse from the Simon et al. (2006a) catalogue is overplotted on 2MASS data (top) and GLIMPSE mid infrared data (bottom). The number of 2MASS stars detected is lower within the ellipse, and the colours of the stars are limited to blue (foreground) and heavily reddened (background). The GLIMPSE data shows a substantial decrease of the 8μ diffuse emission within the ellipse. However the number of point source detections, within completeness limits, is nearly three times higher in the $3.6 \mu\text{m}$ and $4.5 \mu\text{m}$ IRAC bands than in

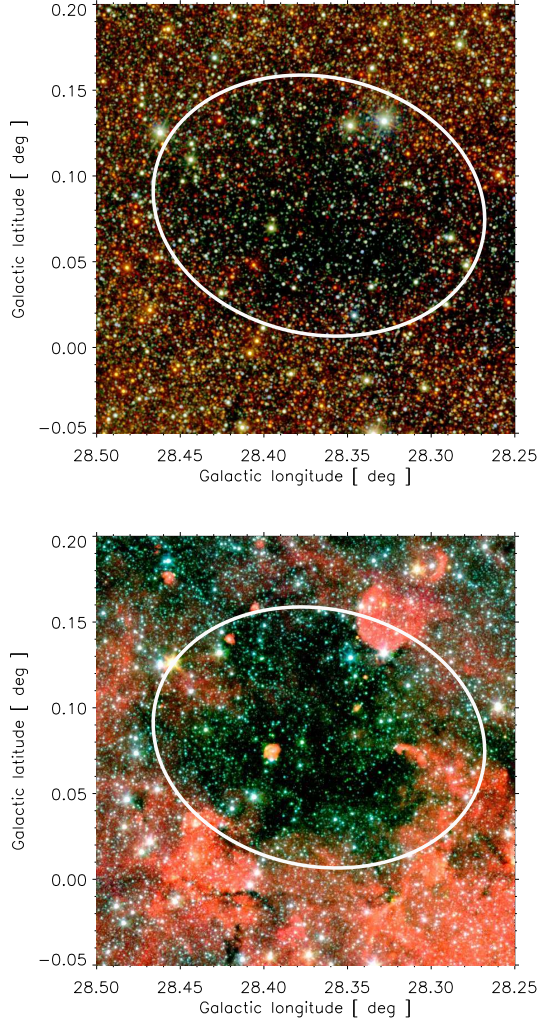


Fig. 3.— Infrared observations towards MSXDC G028.37+00.07 (ellipse). **Top:** Near infrared observations from 2MASS. **Bottom:** Mid infrared observations from Spitzer / GLIMPSE.

the three 2MASS bands. This opens up the possibility of using these longer wavelength observations to conduct a similar study in the future.

To determine the extinction of and distance to an individual cloud, we calculate the derivative of the extinction with respect to distance along the line of sight (i.e. dA_{KS}/dr). This, in effect, gives us the space density of absorbing matter which in our case is dominated by large dust grains (sizes typically of the order of 1

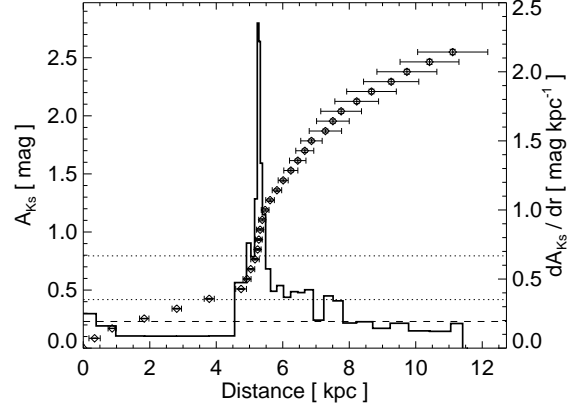


Fig. 4.— Example of cloud detection for MSXDC G028.37+00.07. The diamonds and error bars are as for Fig.1. The solid line is the density of absorbing matter (dA_{KS}/dr), the dashed line is the diffuse extinction and the dotted lines show the diffuse component + 1 and 3 σ . A cloud has been detected at ~ 5.3 kpc with an extinction of ~ 0.9 mag in the K_s band.

μm). The value of dA_{KS}/dr can be converted to n_H (in total hydrogen, in atomic or molecular form, per cubic centimetre) by assuming a conversion factor between extinction and hydrogen column density. However as this requires us to assume such a value, and as it is just a multiplicative factor, we continue to work in units of mag kpc^{-1} in the K_s band.

The line of sight extinction will be the sum of a diffuse extinction upon which is superimposed one or more clouds. To simplify, we modelize this diffuse component as a constant extinction per unit distance, which we choose to be that which minimises the mean absolute deviation (which we will denote σ in the following) of the line of sight density from the diffuse component. As clouds are present along the line of sight, using all the points will of course overestimate the diffuse component. We therefore repeat the calculation by omitting all points with a density above 3σ . This is repeated until the fractional change of diffuse component and σ are less than 2%.

All peaks in dA_{KS}/dr over 3σ above the diffuse component are then considered as a cloud. The extent of the cloud is found by finding the adjoining points which remain 1σ above the diffuse component. The extinction of the cloud is then the increase in the extinction over the cloud minus the diffuse com-

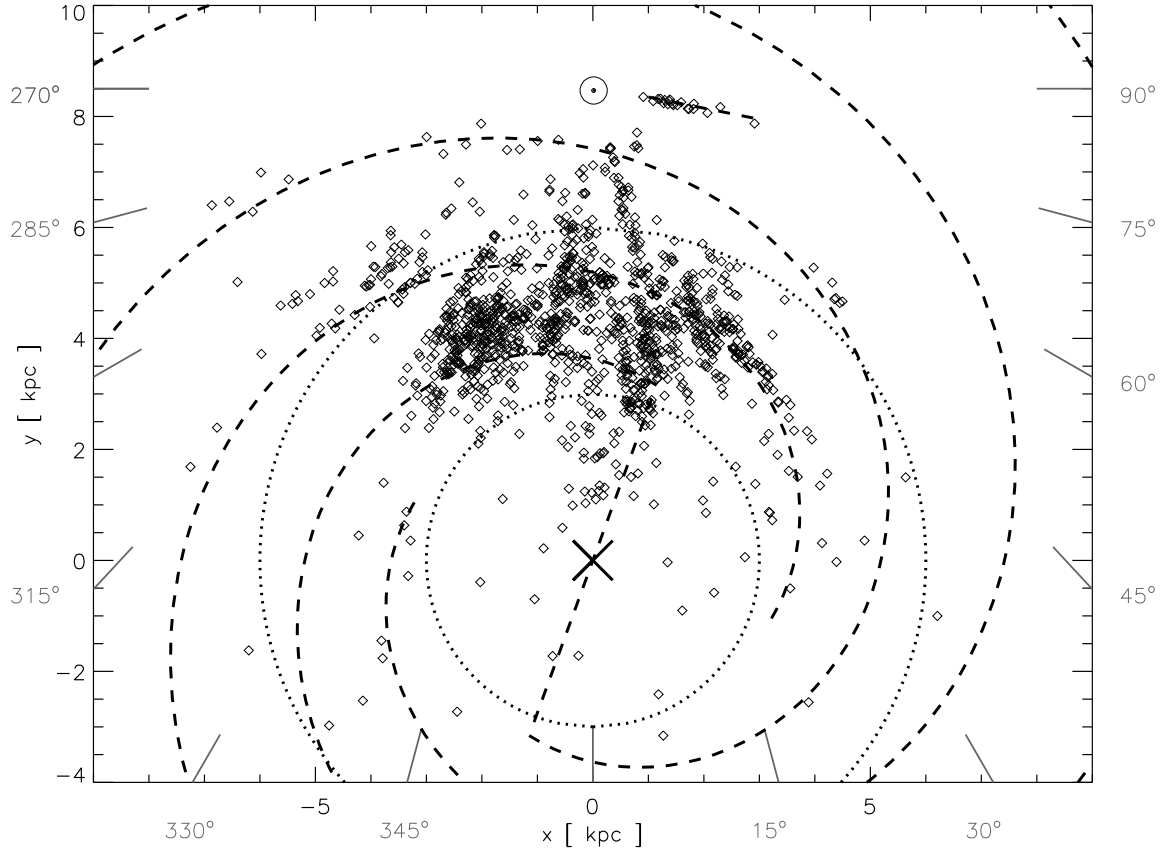


Fig. 5.— Distribution of the IRDCs in the plane of the Galaxy. The dashed lines are the spiral arms from Vallée (2008), the local Orion spur and the Galactic bar. The dotted lines show the Galactocentric distances at 3 and 6 kpc. The IRDCs are seen to be concentrated in the molecular ring ($3 < R < 6$ kpc) and along the spiral arms.

ponent. Only clouds with an extinction over $A_{Ks} \geq 0.114$ are considered, as this threshold corresponds to the density necessary for clouds to be dominated by molecular gas (i.e. $A_V \gtrsim 1$ Spitzer et al. 1973; Binney & Merrifield 1998), if we assume the extinction law of Cardelli et al. (1989). If more than one cloud is found along the line of sight, the one with the largest average extinction is retained as the IRDC. An example line of sight is presented in Fig.4.

Once identified, the distance to the IRDC is simply the density weighted average over the cloud peak:

$$r_{\text{IRDC}} = \frac{\sum_{i=i_{\min}}^{i_{\max}} r_i \times (dA_{Ks}/dr)_i}{\sum_{i=i_{\min}}^{i_{\max}} (dA_{Ks}/dr)_i} \quad (8)$$

The extinction is converted to a column density using the empirical relation between the extinction in the

J band, A_J , and N_H found by Vuong et al. (2003) in ρ Oph dark cloud:

$$N_H = 5.57 \times 10^{21} A_J \text{ cm}^{-2} \text{ mag}^{-1} \quad (9)$$

where N_H is the column density of hydrogen derived from observations of x-ray absorption. We have chosen this value over the more well known Bohlin et al. (1978) relation ($N_H = 1.9 \times 10^{21} A_V \text{ cm}^{-2} \text{ mag}^{-1}$) as the Vuong et al. (2003) result was obtained in a dense star forming region, more similar to the environment that we expect to find in IRDCs. It should be noted, however, that the impact on our mass determinations between the two is only around $\sim 20\%$. As our extinction results are in the Ks band, we adapt the Vuong et al. (2003) relation using the Cardelli et al. (1989) extinction curve ($A_V : A_J : A_{Ks} = 1 : 0.282 : 0.114$).

In order to transform this into a mass, the column

density is multiplied by the area of the cloud and a multiplicative factor of 1.36 (Allen 1973) is applied to take into account the presence of Helium and other heavy elements. The mass of a cloud with area Σ_{IRDC} pc² is then :

$$\frac{M_{\text{IRDC}}}{M_{\odot}} = 150 \times \left(\frac{A_{K_s}}{\text{mag}} \right) \times \left(\frac{\Sigma_{\text{IRDC}}}{\text{pc}^2} \right). \quad (10)$$

This method assumes that the cloud covers the entire ellipse defined in the Simon et al. (2006a) IRDC candidate catalogue. As this is not always the case, this supposition may result in the mass being overestimated. On the other hand, if parts of the cloud completely obscure the NIR light emitted by background stars then the cloud mass will be underestimated. Nevertheless, the resulting mass is expected to be accurate to within a factor of a few.

4. Results

The present method has been applied to over 1500 IRDC candidates (using the selection described above) and we have detected 1259 of them with an $A_V \geq 1$. The use of the genetic algorithm allows us to apply the technique to a lower number of stars than the method published in Marshall et al. (2006), allowing us to probe smaller and denser clouds. As a result, the current method results in a factor of four more cloud detections than the older method. Due to the number of detections, the full table of the IRDC characteristics will only be available electronically, via the Vizier service², but an example of the results is shown in table 1. The distribution of the detected IRDCs in the plane of the Galaxy is displayed in Fig.5. The overlaid spiral arms are from Vallée (2008), with the addition of the local Orion spur. The bar angle plotted here is 20°, in agreement with recent values Gerhard (2002). This spiral structure is not constrained by the distribution of IRDCs presented here, but is overplotted for comparison. The clouds are seen to preferentially lie along the spiral arms of the Galaxy, as well as in the molecular ring ($3 < R < 6$). Also, a concentration of IRDCs is visible at the end of the near side of the Galactic bar. These regions are all associated with high rates of star formation, reinforcing the idea that IRDCs are the precursors to massive stars.

The distribution of the clouds in Galactocentric distance is shown in Fig.6. Few clouds are seen to lie

within 3 kpc of the centre. The bulk of the clouds are concentrated between 3 and 6 kpc, corresponding to the molecular ring. This is reflected in both the 1st and 4th quadrant IRDCs, however there is an asymmetry at $R = 6$ kpc due to the presence of the Carina arm. Furthermore, the local Orion spur is present in the 1st quadrant only, creating a peak at $R \sim 8.5$ kpc. There are more IRDCs in the 4th quadrant, however this may just be due to the presence of more spiral arm tangents in this quadrant, making the detection of IRDCs easier.

The range of masses of the detected IRDCs run from just over ten solar masses up to $8.7 \times 10^4 M_{\odot}$, with an average mass of $\sim 3.5 \times 10^3 M_{\odot}$. Defining their size as the radius of a circle with the same area as the IRDC ellipse, the average size of the IRDCs is ~ 7 pc with the size ranging from a minimum of 0.9 to a maximum of 64 pc. The average extinction is $A_{K_s} \sim 0.35$ mag corresponding to a total hydrogen column density of $\sim 5 \times 10^{21} \text{cm}^{-2}$ while the maximum extinction detected is $A_{K_s} = 1.32$ mag or $\sim 2 \times 10^{22} \text{cm}^{-2}$. As pointed out by Simon et al. (2006b), this range places IRDCs somewhere between the larger, more diffuse giant molecular clouds, and the smaller, denser Bok globules.

The mass spectrum of the IRDCs is estimated by binning the mass distribution into logarithmically spaced bins. The mass spectrum is then calculated from the number of clouds in each bin divided by the size of the bin :

$$f(M) = \frac{dN}{dM} \approx \frac{N_i}{\Delta M_i} \quad (11)$$

where N_i is the number of clouds in bin i and ΔM_i is the size of the i^{th} bin. Mass spectra constructed using binned masses can introduce systematic errors as the slope is sensitive to the choice of the bin size. However, for samples with $N > 500$ the resulting uncertainty in the spectral index is lower than 0.1 (Rosolowsky 2005).

The binned mass spectrum of the IRDCs is displayed in Fig.7. The errors shown do not take into account errors in the mass estimation, and are simply counting errors : $\sigma = \sqrt{N}/\Delta M$. Small clouds are undersampled, due to the relatively large amount of stars necessary to apply the 3D extinction technique, and to the fact that large clouds are much easier to detect at large distances. For masses greater than $\sim 1.7 \times 10^3 M_{\odot}$, the mass spectrum is seen to follow a power law ($f(M) \propto M^{\gamma}$). A straight line fit to the spectrum for $M > 1.7 \times 10^3 M_{\odot}$ yields a spec-

²<http://vizier.u-strasbg.fr/viz-bin/VizieR>

Name	l °	b °	Distance kpc	A_{K_s} mag	Size pc	Mass M_\odot	N_{obs}	χ_r^2	σ
G025.65+00.55	25.6550	0.5590	3.92	0.580	8.94	5768	381	2.43	51.55
G025.66-00.12	25.6690	-0.1260	4.69	0.160	4.57	416	60	0.60	14.11
G025.72-00.28	25.7240	-0.2870	4.85	0.200	4.64	535	65	0.80	32.41
G025.74-00.44	25.7450	-0.4410	4.35	0.180	13.43	4044	726	3.11	9.90
G025.79+00.81	25.7990	0.8150	4.10	1.040	5.96	4594	116	1.26	67.43
G025.85+00.49	25.8530	0.4950	3.98	0.900	6.07	4134	102	1.01	439.74
G025.90+00.33	25.9060	0.3350	4.29	0.470	5.17	1563	100	0.68	41.12
G025.92+00.26	25.9260	0.2660	7.06	0.170	9.38	1864	92	0.67	3.79
G025.94+00.63	25.9420	0.6390	2.63	0.280	3.09	332	134	0.94	11.34
G026.18+00.14	26.1900	0.1500	5.07	0.460	5.20	1547	74	0.97	22.18

Table 1: Example of the results for the IRDC characteristics. For each cloud is listed, in order, it's name, Galactic coordinates l and b , distance, extinction, size, mass, the number of 2MASS stars used in extinction calculation, the reduced χ^2 (Eq.4) and the number of standard deviations the density of the cloud sits above the background (see Fig.3).

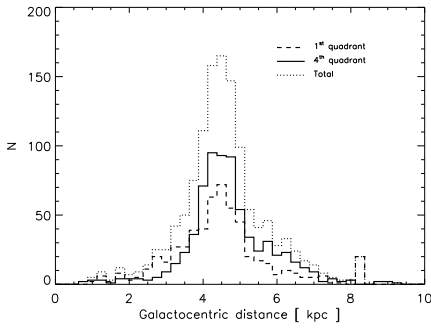


Fig. 6.— Distribution of Galactocentric distances of IRDCs: Dotted line (all clouds), dashed line (1st quadrant) and solid line (4th quadrant). The peak occurs in the molecular ring.

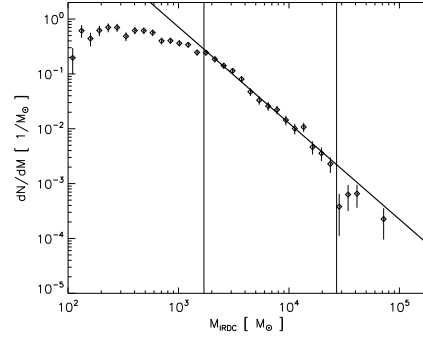


Fig. 7.— Mass spectrum of the IRDCs. After $\sim 1.7 \times 10^3 M_\odot$, the spectrum is well fit by a power law (solid line) with a possible break at high mass. The two vertical lines delimit the zone where the cloud sample is deemed to be complete.

tral index of $\gamma = -1.75 \pm 0.06$ (solid line in Fig.7), steeper than reported values for molecular clouds in the inner Galaxy (Solomon et al. 1987; Rosolowsky 2005) and flatter than the slope found by Simon et al. (2006b) for their IRDC selection. The data seem to suggest that at the highest masses there is a break in the power law. However the average number of clouds per bin at these masses is just over 2, so it is not possible to reach any firm conclusion. These points (to the right of the second vertical line in Fig.7) have not been used in the linear fit. One possible explanation to the high mass cutoff seen may be high mass clouds being mistakenly identified as several smaller mass clouds in IRDC input catalogue, an effect mentioned

by Rosolowsky (2005). In order to tackle this problem, the IRDCs could be characterised using higher resolution MIR observations such as the GLIMPSE survey, which would enable a more robust characterisation of the IRDCs.

Hennebelle & Chabrier (2008) examine the mass spectral index γ of a cloud population governed by density fluctuations induced by turbulence. They find that $\gamma = -2 + (n' - 3)/3$ where n' is the power spectrum index of $\log(\rho)$. They also mention that simulations show n' to be close to the Kolmogorov turbulence index, or $n' \sim 11/3$. This results in a mass

spectral index of $\gamma \sim -1.77$ - very close to what we find. This suggests that the IRDCs in our sample are not virialised but are the result of density fluctuations induced by turbulence. This observation does not exclude the presence of higher density, autogravitating regions within the individual clouds in our IRDC selection. These higher density regions could in fact be completely missed by our method as the column density of the dust would be too high to observe background stars in the near infrared and at the 2MASS completeness limit.

5. Discussion

5.1. Limits of NIR extinction

The main difficulties in using the present method to obtain information on the IRDCs are the small sizes and large densities of the clouds. The technique we employ requires the detection of many stars along the line of sight to obtain enough information on the 3D extinction. This rules out small clouds and clouds so dense that too few stars are detected behind them. Thus, for our initial selection, we start by rejecting all clouds that lie along lines of sight having fewer than 50 stars detected in the three 2MASS bands.

The completeness of the 2MASS catalogue is limited by source confusion, and is a problem in the Galactic plane and towards the Galactic bulge. However, as we are concentrating on high extinction features, source confusion is less of a problem and the 2MASS completeness limit is less severe. In fact, the average completeness in three bands of our IRDC sample is 15.2, 13.9 and 13.1 for the J , H , and K_s bands, respectively. As we use a bright cutoff at magnitude 10, the largest $J - K_s$ observable is 5.2, which results in a maximum extinction of ~ 3.5 in the K_s band and a maximum column density of $5.1 \times 10^{22} \text{ cm}^{-2}$, from Eq. 9. The minimum extinction detectable results from the colour uncertainty in the 2MASS dataset, and corresponds to about $7 \times 10^{20} \text{ cm}^{-2}$. This range of densities is compatible with the typical densities found for IRDCs through ^{13}CO observations (Simon et al. 2006b).

5.2. Comparison with existing measures

Simon et al. (2006b) measured the ^{13}CO line towards over 300 candidate IRDCs in the first Galactic quadrant. They used the radial velocity channels of the CO observations that matched the extinction fea-

tures in the MSX data (Simon et al. 2006a). They then attributed a kinematic distance to the cloud by assuming circular motion and using the Clemens (1985) rotation curve. They solved the inner Galaxy distance ambiguity by assuming that all clouds are at their near kinematic distance as the clouds are seen in extinction and therefore must lie in front of the Galactic background emission. The masses were calculated from the CO emission and by assuming an H_2 to CO conversion factor.

We have detected 107 of their sample using the present method - the other clouds in their study either have too few 2MASS stars detected towards them ($> 75\%$ of their sample) or do not present an extinction feature with $A_V > 1$. For a number of their lines of sight, they include distances for two or more line of sight clouds; we take the highest density cloud to compare with our estimate. The different results for the distances of this IRDC sample are compared on the left side of Fig.8. The black solid line shows equality and the dotted lines are placed at ± 2 kpc from equality. Although there is appreciable scatter, there is general agreement for most of the points. Clouds for which extinction distances differ greatly from the kinematic distances may, in fact, be different clouds. As we have not mapped out the cloud, we are not able to morphologically match the extinction in the NIR to the MIR extinction features as Simon et al. (2006b) do. On the other hand, some of their distances estimates may be wrong due to their systematic choice of the near kinematic distance. On the right hand side of the Fig.8 is the histogram of the difference between the two distance determinations. Here we can see that over 80% of the distance determinations are within 2 kpc of each other. There is only a slight systematic offset of ~ 0.5 kpc.

Jackson et al. (2008) obtained distances for IRDC candidates from the Simon et al. (2006a) sample in the fourth quadrant using observations of the CS molecule. This molecule requires high density for excitation making it a good tracer of dense clouds. Like us, they do not map the clouds but search for the highest density feature along the line of sight. In the centre of Fig.8 we compare our distance measurements to theirs, for the 95 lines of sight where both methods detect a cloud. For a number of their lines of sight, they include distances for two line of sight clouds; we take the higher density cloud to compare with our estimate. There is a systematic offset of around 1.5 kpc between the two methods (Fig.8, right), with just a few points

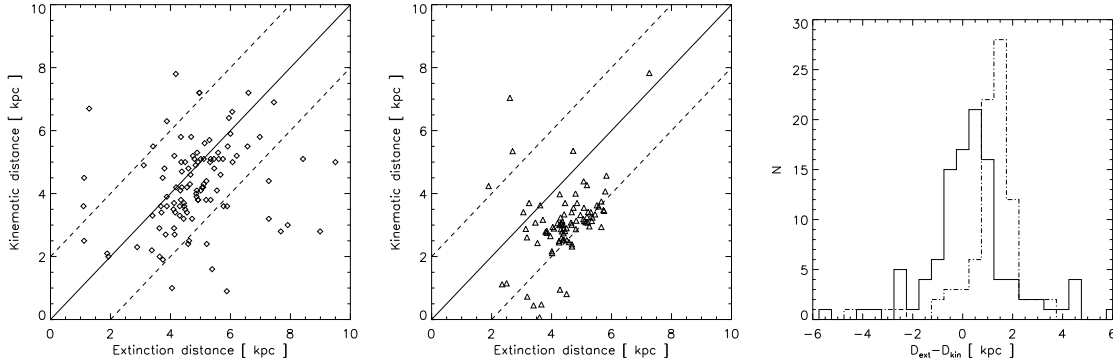


Fig. 8.— **Left** : Scatter plot of extinction distances with the kinematic distances listed in Simon et al. (2006b). The black line shows equality and the dotted lines are at ± 2 kpc. **Middle** : Comparison of extinction distances with the kinematic distances listed in Jackson et al. (2008). **Right** : Histogram of differences between extinction distances and kinematic distances as found by Simon et al. (2006b) (solid line) and Jackson et al. (2008) (broken line). A significant ~ 1.5 kpc systematic difference is found with the distances reported by Jackson et al. (2008).

differing by much more. As mentioned above, these outliers may be due to different line of sight clouds being detected with the two methods or may be due to the systematic choosing of the near kinematic distance by Jackson et al. (2008).

As the mass depends on the square of the distance, the latter is key in determining accurate masses. In Fig. 9 we compare our mass estimates with those from Simon et al. (2006b) (+) and Rathborne et al. (2006) (\diamond). Note that Fig. 9 is a log-log plot. There is appreciably more scatter here compared to that observed for the distances. Most mass estimates agree within a factor of ten and our mass estimates are generally larger than the Rathborne et al. (2006) estimates. Considering the uncertainties in the three methods, an order of magnitude difference between methods is to be expected as the techniques used trace different parts of the IRDCs.

CO observations of IRDCs are a good tracer of the lower density envelope, but may be optically thick towards the denser cores. Also, the low temperatures in the cores may cause the CO molecules to form ice mantles on the dust grains (Alves et al. 1999). Observations of the dust mm-continuum is optically thin, even at the very high column densities of the IRDC cloud cores. On the other hand, current mm observations are more sensitive to the small scale structure but miss out much of the extended emission of the cloud (Bergin & Tafalla 2007). Thus it is not surprising that our mass estimates are closer to those of

Simon et al. (2006b), as our method will also miss out the dense cores while recovering the lower density envelope, and that they are higher than Rathborne et al. (2006) as most of the mass of dark clouds is contained in the lower density envelope (Alves et al. 1999; Cambr sy et al. 2002; Lombardi et al. 2006).

By comparing their results with those from Simon et al. (2006b), Jackson et al. (2008) report an asymmetry in the distribution of 1st quadrant IRDCs compared to 4th ones. Our analysis does not show this asymmetry, however we find that the kinematic distances in the first quadrant have less of an offset to the extinction distances than the fourth quadrant IRDCs. This may be evidence of a difference in the velocity field between the two quadrants, or may be due to a large scale stellar asymmetry not present in the Galactic model. Indeed, results from the Galactic Legacy Mid-Plane Survey Extraordinaire (GLIMPSE Benjamin et al. 2005) show stellar overdensities along a number of lines of sight crossing spiral arm tangencies. However these are present in both the first and fourth quadrants with similar intensities, and so they do not seem to be responsible for introducing such a large bias in our measurements. Furthermore, a number of precise parallax measurements of star forming regions using the NRAO Very Long Baseline Array (VLBA) show very good agreement with the kinematic distances towards massive star forming regions in the first quadrant (Brunthaler et al. 2008; Zhang et al. 2008), although, to our knowledge, no

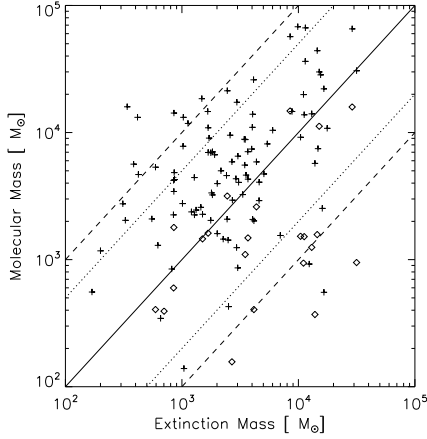


Fig. 9.— Comparison of our mass estimates with those from Simon et al. (2006b)(plus signs) and Rathborne et al. (2006)(diamonds).

similar measurements exist for the fourth quadrant. Kinematic distances in the region studied have uncertainties of 0.5-1.5 kpc and occasionally up to 3 kpc (Gómez 2006) due to non-circular motions associated with the spiral arm shocks. The distance obtained from the 3D extinction has an uncertainty of $\sim 0.5 - 1$ kpc. However, the selection of IRDCs seen in extinction may be polluted by other line of sight clouds.

5.3. Galactic spiral structure

The distribution of IRDCs shown in Fig. 5 is seen to follow the spiral structure of the Galaxy. However, departures are to be seen, especially between the Norma and Scutum arms at Galactocentric distances of between 4 and 5 kpc. This distance matches that of the Molecular ring (Taylor & Cordes 1993; Dame et al. 2001) which may be a ring like structure or may be the result of current angular resolution being unable to resolve multiple spiral arms in this region (Vallée 2008). The spiral pattern traced out by the IRDCs in Fig. 5 could be explained by either an actual molecular ring or the bifurcation of one arm into two. Kinks and wiggles are present in every external spiral galaxy observed, so we are not to expect perfect logarithmic spirals from our own host Galaxy. The current results, however, are not enough to refute or confirm the molecular ring hypothesis, as there may be some (as yet) unknown bias affecting the results in the 4th quadrant.

The current catalogue of IRDC candidates (Simon et al. 2006a) is not a complete survey of cold dark, “IRDC-like”, clouds in the Galaxy. Indeed, it has been compiled with a severe bias - as the clouds are seen in extinction in the MIR, they require a bright background to be detected. As such they are almost exclusively on the near side of the Galaxy and are concentrated at very low Galactic latitudes. With the recent launch of Planck, a full sky survey of sub-millimetre emission from cold dust will soon be accessible. These observations will provide an unbiased survey of the cold cores which are known to be associated with IRDCs. The present 3D extinction method could be adapted to probe these higher density cores by utilising stellar MIR observations, such as the GLIMPSE survey (see Fig.3), or the upcoming all sky MIR survey “Wide-field Infrared Survey Explorer” (WISE, Duval et al. 2004).

Compared to kinematic distances, the 3D extinction method has the advantage of providing temperature independent measures of the dust column density, as well as avoiding the near - far distance ambiguity which plagues kinematic distance estimates within the solar circle. By using the MIR observations mentioned previously, along with the deep NIR observations of the Galactic Plane from the “UKIRT Infrared Digital Sky Survey (Galactic Plane Survey)” (UKIDSS(GPS), Lucas et al. 2008), it will be possible to map out the spiral structure of our Galaxy to the far side of the solar circle and perhaps beyond.

6. Conclusions

We have applied a new three dimensional extinction technique towards over 1500 IRDC cloud candidates, for which we recovered distances and masses for 1259 of them, including over 1000 previously unmeasured clouds. This is a much larger sample than previous studies, enabling the study of the cloud population as a whole. The spatial distribution of the clouds is found to be concentrated in the molecular ring and along the spiral arms, reinforcing the idea that IRDCs are the birthplace for high mass stars. Their mass spectrum follows a power law with a slope of -1.75 ± 0.06 which is steeper than GMCs in the inner Galaxy, similar to CO clumps and shallower than molecular cores or the stellar IMF. This slope suggests that the IRDC population is composed of non-gravitationally bound clouds, and are the result of density fluctuations induced by turbulence. However, higher density auto-

gravitating clumps inside the individual clouds of our IRDC selection would most likely be missed by the present method.

This new method is independent of any kinematical information, thus providing a new way to obtain information on the Galactic distribution of the ISM. It is a good complement to existing measures which are solely based on molecular gas kinematics as both methods are completely independent and both are affected by different systematics. It will be able to provide valuable distance information for use in the analysis and interpretation of far-infrared and sub-millimetre observations by Herschel and Planck. In the future it could be used with deeper stellar observations or observations at longer wavelengths in order to probe even higher density clouds and to even larger distances.

We would like to thank P.Hennebelle, G.Chabrier and M.Miville-Deschenes for helpful discussions. The anonymous referee provided a detailed report which helped improve the quality and clarity of the text. D.J.Marshall was funded by the Natural Sciences and Engineering Research Council of Canada through its SRO programme. This publication makes use of data products from the Two Micron All Sky Survey, which is a joint project of the University of Massachusetts and the Infrared Processing and Analysis Center/California Institute of Technology, funded by the National Aeronautics and Space Administration and the National Science Foundation. The CD-SClient package was used for the remote querying of the 2MASS dataset. *Facilities:* 2MASS

REFERENCES

- Allen, C. W. 1973, *Astrophysical quantities* (London: University of London, Athlone Press, 3rd ed.)
- Alves, J., Lada, C. J., & Lada, E. A. 1999, *ApJ*, 515, 265
- Bellazzini, M., Ibata, R., Monaco, L., Martin, N., Irwin, M. J., & Lewis, G. F. 2004, *MNRAS*, 354, 1263
- Benjamin, R. A. et al. 2005, *ApJ*, 630, L149
- Bergin, E. A., & Tafalla, M. 2007, *ARA&A*, 45, 339
- Binney, J., & Merrifield, M. 1998, *Galactic astronomy* (Princeton University Press)
- Bohlin, R. C., Savage, B. D. & Drake, J. F. 1978, *ApJ*, 224, 132
- Brunthaler, A., Reid, M. J., Menten, K. M., Zheng, X. W., Moscadelli, L., & Xu, Y. 2008, *ArXiv e-prints*
- Cambr  sy, L., Beichman, C. A., Jarrett, T. H., & Cutri, R. M. 2002, *AJ*, 123, 2559
- Cardelli, J.A., Clayton, G.C. & Mathis, J.S. 1989, *ApJ*...345..245
- Chambers, E.T., Jackson, J.M., Rathborne, J.M. and Simon, R. 2009, *ApJS*, 181, 360
- Charbonneau, P. 1995, *ApJS*, 101, 309
- Clemens, D. P. 1985, *ApJ*, 295, 422
- Dame, T. M., Hartmann, D., & Thaddeus, P. 2001, *ApJ*, 547, 792
- Duval, V.G., Irace, W.R., Mainzer, A.K. & Wright, E.L. 2004, *SPIE*, 5487, 101
- Egan, M. P., Shipman, R. F., Price, S. D., Carey, S. J., Clark, F. O., & Cohen, M. 1998, *ApJ*, 494, L199+
- Froebrich, D., & del Burgo, C. 2006, *MNRAS*, 369, 1901
- Gerhard, O. 2002, *ASP Conf. Ser.* 273, 73
- Gieles, M., Larsen, S. S., Scheepmaker, R. A., Bastian, N., Haas, M. R., & Lamers, H. J. G. L. M. 2006, *A&A*, 446, L9
- G  mez, G. C. 2006, *AJ*, 132, 2376
- Hennebelle, P. & Chabrier, G. 2008, *A&A*
- Indebetouw, R. et al. 2005, *ApJ*, 619, 931
- Jackson, J. M., Finn, S. C., Rathborne, J. M., Chambers, E. T., & Simon, R. 2008, *ApJ*, 680, 349
- Larsen, S. S. 2008, *A&A*, In press
- Lombardi, M., Alves, J., & Lada, C. J. 2006, *A&A*, 454, 781
- Lucas, P. W. et al. 2008, *MNRAS*, 391, 136
- Marshall, D. J., Robin, A. C., Reyl  , C., Schultheis, M., & Picaud, S. 2006, *A&A*, 453, 635
- Mathis, J. S. 1990, *ARA&A*, 28, 37

- Momany, Y., Zaggia, S. R., Bonifacio, P., Piotto, G., De Angeli, F., Bedin, L. R., & Carraro, G. 2004, *A&A*, 421, L29
- Ormel, C. W., Shipman, R. F., Ossenkopf, V., & Helmich, F. P. 2005, *A&A*, 439, 613
- Perault, M. 1996, *A&A*, 315, L165
- Picaud, S., Cabrera-Lavers, A., & Garzon, F. 2003, *A&A*, 408, 141
- Picaud, S., & Robin, A. C. 2004, *A&A*, 428, 891
- Pillai, T., Wyrowski, F., Menten, K. M., & Krugel, E. 2006, *A&A*, 447, 929
- Press, W. H., Teukolsky, S. A., Vetterling, W. T., & Flannery, B. P. 1992, *Numerical recipes in FORTRAN. The art of scientific computing* (Cambridge: University Press, 2nd ed.)
- Price, S. D. 1995, *Space Science Reviews*, 74, 81
- Rathborne, J. M., Jackson, J. M., Chambers, E. T., Simon, R., Shipman, R., & Frieswijk, W. 2005, *ApJ*, 630, L181
- Rathborne, J. M., Jackson, J. M., & Simon, R. 2006, *ApJ*, 641, 389
- Reyle, C., Marshall, D. J., Robin, A. C., & Schultheis, M. 2009, *A&A*, 495, 819
- Robin, A. C., Reyl  , C., Derri  re, S., & Picaud, S. 2003, *A&A*, 409, 523
- Rosolowsky, E. 2005, *PASP*, 117, 1403
- Simon, R., Jackson, J. M., Rathborne, J. M., & Chambers, E. T. 2006a, *ApJ*, 639, 227
- Simon, R., Rathborne, J. M., Shah, R. Y., Jackson, J. M., & Chambers, E. T. 2006b, *ApJ*, 653, 1325
- Skrutskie, M. F. et al. 2006, *AJ*, 131, 1163
- Solomon, P. M., Rivolo, A. R., Barrett, J., & Yahil, A. 1987, *ApJ*, 319, 730
- Spitzer, L., Drake, J. F., Jenkins, E. B., Morton, D. C., Rogerson, J. B., & York, D. G. 1973, *ApJ*, 181, L116+
- Taylor, J. H., & Cordes, J. M. 1993, *ApJ*, 411, 674
- Vall  e, J. P. 2008, *AJ*, 135, 1301
- Vuong, M. H., Montmerle, T., Grosso, N., Feigelson, E. D., Verstraete, L., & Ozawa, H. 2003, *A&A*, 408, 581
- Williams, J. P., & McKee, C. F. 1997, *ApJ*, 476, 166
- Zhang, B., Zheng, X. W., Reid, M. J., Menten, K. M., Xu, Y., Moscadelli, L., & Brunthaler, A. 2008, *ArXiv e-prints*